AMERICAN SOCIETY FOR MICROBIOLOGY | mBio®

RESEARCH ARTICLE

A Novel Aquaporin Subfamily Imports Oxygen and Contributes to Pneumococcal Virulence by Controlling the Production and Release of Virulence Factors

Qingqing Hu,[a,b] Huichun Tong,[a,b] Jing Wang,[c] Pupu Ge,[c,d] Lin Zhu,[a,b] Cuihua Liu,[c,d] Jing-ren Zhang,[e] Xiuzhu Dong[a,b]

[a]State Key Laboratory of Microbial Resources, Institute of Microbiology, Chinese Academy of Sciences, Beijing, China
[b]University of Chinese Academy of Sciences, Beijing, China
[c]CAS Key Laboratory of Pathogenic Microbiology and Immunology, Institute of Microbiology, Center for Biosafety Mega-Science, Chinese Academy of Sciences, Beijing, China
[d]Savaid Medical School, University of Chinese Academy of Sciences, Beijing, China
[e]Center for Infectious Disease Research, School of Medicine, Tsinghua University, Beijing, China

Qingqing Hu and Huichun Tong contributed equally. Author order was determined by alphabetical order.

ABSTRACT Aquaporins, integral membrane proteins widely distributed in organisms, facilitate the transport of water, glycerol, and other small uncharged solutes across cellular membranes and play important physiological roles in eukaryotes. However, characterizations and physiological functions of the prokaryotic aquaporins remain largely unknown. Here, we report that *Streptococcus pneumoniae* (pneumococcus) AqpC (Pn-AqpC), representing a new aquaporin subfamily possessing a distinct substrate-selective channel, functions as an oxygen porin by facilitating oxygen movement across the cell membrane and contributes significantly to pneumococcal virulence. The use of a phosphorescent oxygen probe showed that Pn-AqpC facilitates oxygen permeation into pneumococcal and Pn-AqpC-expressing yeast cells. Reconstituting Pn-AqpC into liposomes prepared with pneumococcal and *Escherichia coli* cellular membranes further verified that Pn-AqpC transports O_2 but not water or glycerol. Alanine substitution showed that Pro232 in the substrate channel is key for Pn-AqpC in O_2 transport. The deletion of Pn-*aqpC* significantly reduced H_2O_2 production and resistance to H_2O_2 and NO of pneumococci, whereas low-H_2O_2 treatment helped the ΔPn-*aqpC* mutant resist higher levels of H_2O_2 and even NO, indicating that Pn-AqpC-facilitated O_2 permeation contributes to pneumococcal resistance to H_2O_2 and NO. Remarkably, the lack of Pn-*aqpC* alleviated cell autolysis, thus reducing pneumolysin (Ply) release and decreasing the hemolysis of pneumococci. Accordingly, the ΔPn-*aqpC* mutant markedly reduced survival in macrophages, decreased damage to macrophages, and significantly reduced lethality in mice. Therefore, the oxygen porin Pn-AqpC, through modulating H_2O_2 production and pneumolysin release, the two major pneumococcal virulence factors, controls the virulence of pneumococcus. Pn-AqpC orthologs are widely distributed in various pneumococcal serotypes, highlighting that the oxygen porin is important for pneumococcal pathogenicity.

IMPORTANCE Pneumococcus is the leading cause of community-acquired pneumonia, bacteremia, and meningitis. This work reports that a novel aquaporin subfamily represented by pneumococcal Pn-AqpC functions as an oxygen porin facilitating O_2 influx into cells. Importantly, by mediating O_2 influx, Pn-AqpC controls the production and release of H_2O_2 and Ply, the two major pneumococcal virulence factors. Moreover, by enhancing endogenous H_2O_2 production, Pn-AqpC significantly increases pneumococcal resistance to H_2O_2 and even NO, the major bactericidal chemical produced by macrophages. Consequently, the deletion of Pn-*aqpC* markedly decreased pneumococcal survival in macrophages and reduced damage to macrophages. Accordingly, the ΔPn-

Citation Hu Q, Tong H, Wang J, Ge P, Zhu L, Liu C, Zhang J, Dong X. 2021. A novel aquaporin subfamily imports oxygen and contributes to pneumococcal virulence by controlling the production and release of virulence factors. mBio 12:e01309-21. https://doi.org/10.1128/mBio.01309-21.

Editor Joanna B. Goldberg, Emory University School of Medicine

Address correspondence to Huichun Tong, tonghuichun@im.ac.cn, or Xiuzhu Dong, dongxz@im.ac.cn.

Received 11 June 2021
Accepted 12 July 2021
Published 17 August 2021

aqpC mutant displays significantly attenuated virulence in a murine pneumonia model. Given that Pn-AqpC orthologs are widely distributed in all pneumococcal serotypes, this new subfamily of aquaporins is identified as novel virulence-related proteins.

KEYWORDS *Streptococcus pneumoniae*, oxygen-transporting aquaporin, new subfamily of aquaporins, hydrogen peroxide production, ROS and RNS resistance, pneumolysin release, survival in macrophages, virulence

Streptococcus pneumoniae (pneumococcus) is a major cause of community-acquired pneumonia, bacteremia, and meningitis (1, 2). It relies on multiple virulence factors, capsular polysaccharides (CPSs), pneumolysin (Ply), and H_2O_2, to transmit and escape the host's innate immune system (1, 3–5). Distinguishingly, pneumococcus produces as well as resists high concentrations of H_2O_2 (6, 7). The ability to resist oxidative stress enables pneumococcus to survive against killing by host phagocytes (8, 9); particularly, intramacrophage survival is key to effective septic infection by pneumococcus (10). However, excess endogenous H_2O_2 also imposes oxidative stress on pneumococcus (11); therefore, effective efflux of H_2O_2 would be a way for detoxification. Recently, an aquaporin of *Streptococcus oligofermentans*, a close relative of pneumococcus, was reported to facilitate the efflux of cellular H_2O_2 (12). This provides a clue that pneumococcus may also employ aquaporins not only for the efflux of H_2O_2 for detoxification but also for virulence.

Aquaporins are integral membrane proteins found in diverse organisms (13–15). They facilitate the diffusion of water, glycerol, H_2O_2, ammonia, and other small uncharged solutes across cellular membranes and play important roles in physiological activities and diseases in eukaryotes (13, 15–19). Aquaporins are categorized into three major phylogenetic subfamilies: the classical water-transporting aquaporins (AQPs), the glycerol-transporting aquaglyceroporins (AQGPs), and the AQP supergene channel superaquaporins (SAQPs) (14). The three aquaporin subfamilies differ in their amino acid compositions of the aromatic/arginine constriction region (ar/R region), also known as the selective filter (20). However, only a few prokaryotic aquaporins have been studied regarding their physiological functions (21, 22).

Unexpectedly, we found that pneumococcus and some streptococcal pathogenic species encode a distinct aquaporin ortholog distantly related to the *Escherichia coli* glycerol facilitator GlpF, thus possibly representing a new aquaporin subfamily, which is tentatively assigned to the atypical aquaglyceroporins. Through the combination of physiological, biochemical, genetic, and pathogenicity assays, we demonstrated that pneumococcal AqpC (Pn-AqpC), a representative of the new aquaporin subfamily, facilitates O_2 influx into pneumococcal and Pn-AqpC-expressing yeast cells and reconstituted proteoliposomes, thus functioning as an oxygen porin. By transporting O_2, Pn-AqpC promoted pneumococcal H_2O_2 production, resistance to reactive oxygen species (ROS) and reactive nitrogen species (RNS), as well as the release of Ply, an important pneumococcal virulence factor (23). Importantly, Pn-AqpC elevated pneumococcal survival in macrophages and increased damage to macrophages, thus contributing significantly to pneumococcal pathogenicity in a murine pneumonia model. Pn-*aqpC* orthologs are widely distributed in all pneumococcal serotypes and capsule-free strains, implying that this oxygen porin could be a novel virulence-related protein.

RESULTS

Pneumococcus possesses an atypical aquaglyceroporin, Pn-AqpC, representing a novel aquaporin subfamily. Using the *S. oligofermentans* aquaporin So-AqpA (I872_01445) as a probe to query the genome of *S. pneumoniae* D39, an encapsulated serotype 2 strain, three genes (SPD_1320, SPD_1569, and SPD_2011) were hits at amino acid identities of 26%, 95%, and 31%, respectively. Phylogenetically, SPD_1569 clustered with So-AqpA and the water-facilitating aquaporin AqpZ of *E. coli* and thus was assigned as Pn-AqpA; SPD_2011 was clustered with the glycerol facilitator GlpF of *E. coli* and assigned as Pn-AqpB. However, SPD_1320 and some glycerol facilitators

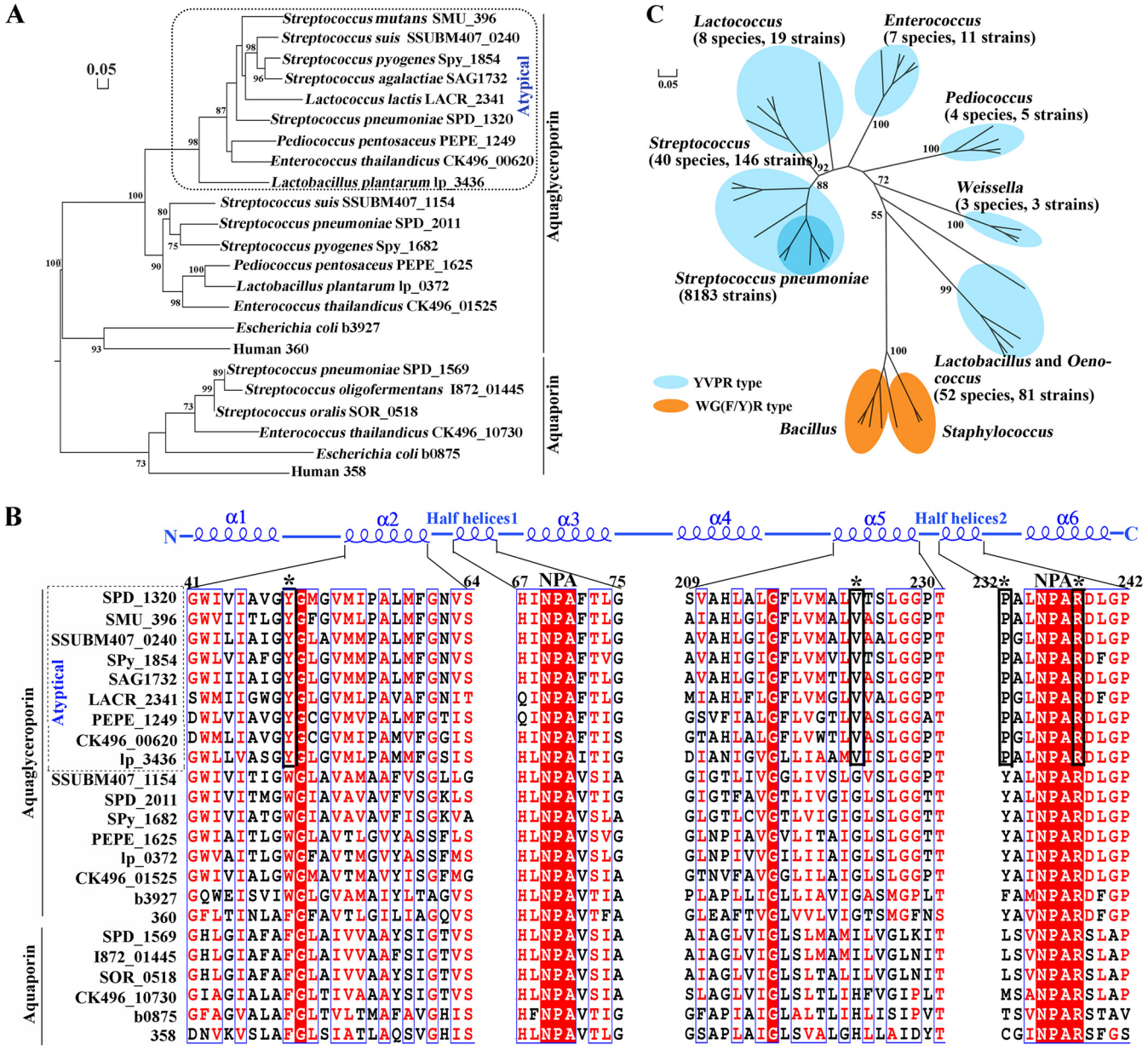

FIG 1 Phylogenetic analysis identifies a new subfamily of aquaporins with unique substrate-selective residues. (A) A phylogenetic tree based on the amino acid sequences of the aquaporin orthologs was constructed using the maximum likelihood method with 1,000 replicates. The bar of 0.05 represents evolutionary distance. A dotted line frames the new subfamily of aquaporins (atypical). (B) The amino acid sequences of the aquaporins in panel A were aligned using ClustalW. The *E. coli* GlpF (b3927) secondary structure (top panel) and the amino acid positions of D39 Pn-AqpC (SPD_1320) (top row of the bottom panel) are shown. Asterisks specify the ar/R region residues, and black lines frame YVPR of the atypical aquaglyceroporins. (C) Distribution of the new subfamily of aquaporins among *Lactobacillales*. Phylogenetic analysis was implemented as described above for panel A on at most five protein sequences of each genus. Numbers inside parentheses are those containing the YVPR-type aquaglyceroporins; branches within the dark blue pie represent pneumococcal strains.

from other lactic acid bacteria clustered to form a separate branch distantly related to *E. coli* GlpF (Fig. 1A) and thus assigned as Pn-AqpC. Aquaporins in the Pn-AqpC-affiliated branch were tentatively named atypical aquaglyceroporins and could represent a new aquaporin subfamily. These aquaporins congruously possess YVPR as the substrate-selective residues (Fig. 1B; see also Fig. S1 in the supplemental material), which are distinct from F(H/I)XR in the water-transporting and WG(F/Y)R in glycerol-transporting aquaporins (Fig. 1B and C). Furthermore, the ar/R region diameter size in each Pn-AqpC monomer (Fig. S2A and B) was between those of the *E. coli* water (Fig. S2C)- and glycerol (Fig. S2D)-transporting aquaporins, implying a different substrate spectrum.

Therefore, we investigated the physiological functions of Pn-AqpC, a representative of the new aquaporin subfamily.

The absence of Pn-*aqpC* reduces H_2O_2 production but promotes the aerobic growth of pneumococcus. To probe the physiological functions of Pn-AqpC, Pn-*aqpC* was deleted in *S. pneumoniae* D39 and its nonencapsulated mutant R6. By reference to *S. oligofermentans* So-AqpA that facilitates H_2O_2 permeation, the function of Pn-AqpC in H_2O_2 transport was first evaluated in R6 and its ΔPn-*aqpC* mutant carrying a specific cellular H_2O_2 reporter HyPer gene (24). However, the HyPer reporter detected similar H_2O_2 influx into ΔPn-*aqpC* and wild-type (WT) cells when provided exogenous H_2O_2 (Fig. S3A, bottom), thus excluding a role of Pn-AqpC in H_2O_2 permeation, whereas significantly lower fluorescence was found in ΔPn-*aqpC* cells when no exogenous H_2O_2 was provided (Fig. S3A, top), indicating reduced H_2O_2 production when Pn-AqpC is absent.

Next, the H_2O_2 yields of the R6 and D39 wild-type strains and ΔPn-*aqp*C mutants were assayed in static cultures of 20 and 30 ml of brain heart infusion (BHI) broth in 100-ml flasks, respectively, which build gradient dissolved O_2 levels. Surprisingly, the two ΔPn-*aqpC* mutants both achieved better growth and lower H_2O_2 yields than the wild-type strains in the two culture volumes (Fig. 2A), while the Pn-*aqpC*-complemented strains (Pn-*aqpC*-com) recovered the wild-type phenotype (Fig. 2A). This suggested that Pn-AqpC might facilitate the transmembrane diffusion of O_2, a substrate for H_2O_2 formation. As similarly reduced cellular H_2O_2 and elevated aerobic growth were determined for the ΔPn-*aqpC* mutants of the nonencapsulated R6 and encapsulated D39 strains, the Pn-*aqpC* deletion-caused phenotype changes may not be related to the capsular polysaccharides; thus, strain R6 was investigated for the physiological functions *per se* of Pn-AqpC in the following experiments, except for animal studies.

Pneumococcal Pn-AqpC facilitates O_2 transport into cells. To verify the function of Pn-AqpC in transporting O_2, a dissolved oxygen microsensor Oxy meter (Unisense, Denmark) was used to measure the residual O_2 contents in stationary-phase cultures of pneumococci growing in 40 ml BHI broth in a 50-ml centrifuge tube, and 1.5- to 1.6-fold-lower O_2 consumption was determined for the R6 ΔPn-*aqpC* mutant than for the wild-type and Pn-*aqpC*-com strains (Fig. 2B). Similarly, using a phosphorescent oxygen probe, a 2.6-fold-lower O_2 uptake rate within 3 min was determined for the ΔPn-*aqpC* mutant than for the wild-type strain, while the Pn-*aqpC*-com strain recovered O_2 uptake levels of the wild type (Fig. 2C). Of note, the H_2O_2 yields in the wild type ($122 \pm 3\,\mu$M) and the ΔPn-*aqpC* mutant ($18 \pm 2\,\mu$M) were much lower than the theoretical stoichiometry ($258\,\mu$M and $173\,\mu$M) calculated from the Oxy meter-measured oxygen consumption in the corresponding strains ($258 \pm 10\,\mu$M and $173 \pm 21\,\mu$M). This indicates that other O_2 consumption pathways are present, such as NADH oxidase (Nox) catalyzing the oxidization of NADH to NAD^+ and H_2O by using O_2 as an electron acceptor (25). Therefore, we deleted *nox* in the wild type and the ΔPn-*aqpC* mutant, which reduced O_2 consumption by 30 ± 3.5 and $34 \pm 5.8\,\mu$M, respectively. Nevertheless, there should have been other unknown pathways consuming the remaining $106\,\mu$M and $121\,\mu$M O_2 in the wild type and the ΔPn-*aqpC* mutant, respectively. Moreover, Pn-*aqpC* deletion did not alter the expression of *spxB* and *lctO*, which encode the two major H_2O_2 production enzymes pyruvate oxidase and lactate oxidase, respectively (Fig. S4). This indicates that the reduced H_2O_2 production in the ΔPn-*aqpC* mutant was due to decreased O_2 influx instead of reduced expression of the H_2O_2 production genes.

The O_2-facilitating function of Pn-AqpC was further verified by the coexpression of Pn-*aqpC* and the sperm whale myoglobin (Mb) gene in *Saccharomyces cerevisiae* INVSc1. Single-Mb-gene-expressing INVSc1-myo and INVSc1 strains were used as controls. In addition, an INVSc1-Pn-*aqpC-gfp* strain carrying a super folder green fluorescent protein (GFP) gene (s*fgfp*) fusion to Pn-*aqpC* was constructed. The expressions of Pn-AqpC and Mb in *S. cerevisiae* were verified by Western blotting (Fig. S5A), and the cytoplasmic membrane localization of heterologously expressed Pn-AqpC in *S. cerevisiae* was confirmed via confocal microscopy examination (Fig. S5B). By measuring the characteristic oxymyoglobin (MbO_2) absorption at 541 nm in yeast protoplasts (26) (Fig. S5C) and purified MbO_2 (Fig. S5D), a significant MbO_2 increase (ΔA_{541}/optical

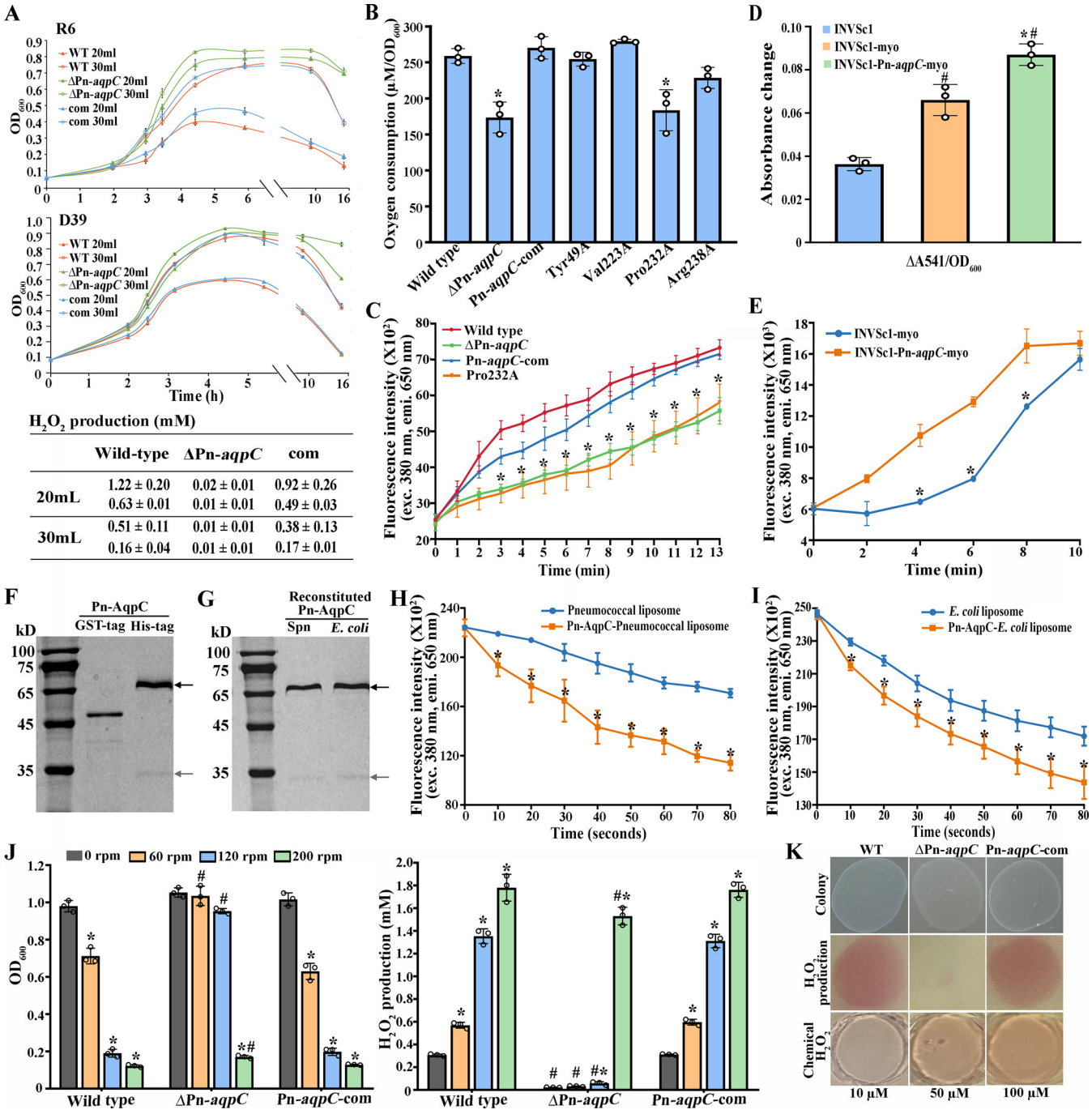

H_2O_2 production (mM)

	Wild-type	ΔPn-*aqpC*	com
20mL	1.22 ± 0.20	0.02 ± 0.01	0.92 ± 0.26
	0.63 ± 0.01	0.01 ± 0.01	0.49 ± 0.03
30mL	0.51 ± 0.11	0.01 ± 0.01	0.38 ± 0.13
	0.16 ± 0.04	0.01 ± 0.01	0.17 ± 0.01

FIG 2 Pneumococcal Pn-AqpC acts as an oxygen porin. (A) Growth of R6 (top) and D39 (bottom) wild-type (WT), ΔPn-*aqpC*, and Pn-*aqpC*-complemented (com) strains cultured statically in 20 and 30 ml of BHI broth in a 100-ml flask. H_2O_2 (millimolar) accumulations in the stationary-phase cultures are listed in the table at the bottom, with those of strains R6 and D39 in the top and bottom rows, respectively. (B) An oxygen microsensor Oxy meter was used to measure the residual dissolved O_2 in the stationary-phase cultures of the R6 wild type and its derivatives grown in 40 ml BHI broth in a 50-ml centrifuge tube. Oxygen consumption per OD_{600} of cell mass was calculated by comparison to 283 μM O_2 in fresh medium. *, significantly different from other strains. (C) Mid-exponential-phase cultures of the R6 wild type and its derivatives were exposed to air, and the residual O_2 in the culture was measured using a phosphorescent oxygen probe. *, significantly different from the wild-type and Pn-*aqpC*-complemented strains. (D) Protoplasts of *S. cerevisiae* INVSc1 and INVSc1 carrying the myoglobin gene (INVSc1-myo) or coexpressed with Pn-*aqpC* (INVSc1-Pn-*aqpC*-myo) were exposed to air, and the A_{541} increase per unit of biomass ($\Delta A_{541}/OD_{600}$) was calculated. (E) The residual O_2 contents in the culture were determined using a phosphorescent oxygen probe. # and *, significantly different from INVSc1 and INVSc1-myo, respectively. (F and G) The recombinant GST–Pn-AqpC–10×His protein was purified (GST-tag), digested with 100 U thrombin to remove the GST tag to obtain Pn-AqpC–10×His (His-tag) (F), and reconstituted into pneumococcal (Spn) and *E. coli* liposomes (G). The Pn-AqpC proteins were examined on a 12% SDS-PAGE gel. The protein ladder is shown at the left. Black and gray arrows indicate the macromolecular aggregate and monomer of Pn-AqpC protein, respectively. (H and I) Pn-AqpC facilitating O_2 permeation across pneumococcal liposomes (H) and *E. coli* liposomes (I) was determined using a phosphorescent oxygen probe. *, the fluorescence intensity change at the respective time points was significantly different from that of the Pn-AqpC-devoid liposomes. (J) The R6 wild-type, ΔPn-*aqpC*, and Pn-*aqpC*-complemented (Pn-*aqpC*-com) strains were cultured

(Continued on next page)

density at 600 nm [OD_{600}]) was found in Pn-*aqpC*-expressing yeast compared to Pn-*aqpC*-devoid INVSc1 (Fig. 2D). Accordingly, the phosphorescent oxygen probe detected a more rapid decrease of the cultural O_2 content of INVSc1-Pn-*aqpC*-myo than that of INVSc1-myo (Fig. 2E). These results collectively showed that Pn-AqpC facilitates oxygen permeation.

Pn-AqpC facilitates oxygen transport across proteoliposomes. To further confirm that Pn-AqpC facilitates the transport of O_2 and other substrates, the recombinant glutathione *S*-transferase (GST)–Pn-AqpC–10×His protein was purified in the detergent octylglucoside (OG), and the GST tag was then removed (Fig. 2F). Two Pn-AqpC–10×His protein bands of ~32 kDa and ~68 kDa were identified as Pn-AqpC by liquid chromatography-tandem mass spectrometry (LC-MS/MS) analysis (Fig. 2F and G; Table S1). Compared to the *E. coli* AqpZ tetramers that hardly dissociated with 1% SDS due to the strong hydrophobic characteristics (27), the 68-kDa protein was assumed to be a macromolecular aggregate, while the 32-kDa protein was assumed to be a monomer. The purified Pn-AqpC–10×His protein was reconstituted into the membrane lipid of pneumococci and *E. coli* (Fig. 2G). The phosphorescent oxygen probe was then wrapped within the proteoliposomes and Pn-AqpC-devoid liposomes to detect oxygen contents. This detected 3.2- and 1.5-fold-higher O_2 influx in the first 40 s into the pneumococcal and *E. coli* proteoliposomes than the respective Pn-AqpC-devoid liposomes, respectively (Fig. 2H and I). Notably, 3-fold-higher O_2 influx was determined for Pn-AqpC-devoid *E. coli* than for the pneumococcal liposomes within 80 s (Fig. 2H and I). These results demonstrated that Pn-AqpC sped up O_2 permeation across the cellular membrane, and the pneumococcal membrane appears to have lower O_2 permeability than that of *E. coli*.

Using a stopped-flow apparatus, Pn-AqpC facilitating water and glycerol permeation was measured based on osmosis-driven permeability. However, similar initial rates (*k*) were determined for proteoliposomes and Pn-AqpC-devoid liposomes in water and glycerol permeation (Fig. S3B to E). Therefore, Pn-AqpC specifically facilitates the permeation of O_2 but not water or glycerol.

Pn-AqpC acts as a prominent oxygen facilitator under lower oxygen levels. Given that O_2, particularly at higher concentrations, permeates freely through the cytoplasmic membrane, the range of O_2 levels wherein Pn-AqpC plays a role in facilitating O_2 was tested by growing the R6 wild-type, ΔPn-*aqpC* mutant, and Pn-*aqpC*-com strains under gradient shaking speeds. Although the three strains exhibited similar growth rates under static and 200-rpm shaking conditions, the ΔPn-*aqpC* mutant grew slightly and markedly better under 60- and 120-rpm shaking conditions (Fig. 2J, left). Accordingly, significantly lower levels of H_2O_2 were produced in the ΔPn-*aqpC* mutant cultured under static, 60-rpm, and 120-rpm conditions, but similar H_2O_2 levels were generated in 200-rpm shaking cultures of wild-type, ΔPn-*aqpC* mutant, and Pn-*aqpC*-com strains (Fig. 2J, right). This shows that Pn-AqpC exerts an O_2 facilitator role when the bacterium lives under lower O_2 levels. Next, the role of Pn-AqpC in the H_2O_2 production of pneumococci under 5% O_2 was tested by mimicking the O_2 concentrations in the human lower respiratory tract within the mucus layer or in close contact with pulmonary epithelial cells (11). The same amounts of the wild-type, ΔPn-*aqpC* mutant, and Pn-*aqpC*-com cultures were spotted onto a BHI agar plate and incubated in an O_2 control *in vitro* glove box (Coy Laboratory Products). Compared with the wild-type and complemented strains, the ΔPn-*aqpC* mutant produced almost undetectable H_2O_2 under 5% O_2 (Fig. 2K); therefore, Pn-AqpC could play an important role in pneumococcal infection by facilitating O_2 import for H_2O_2 production, one of the pneumococcal virulence factors.

FIG 2 Legend (Continued)

with shaking at different speeds. The optical density at 600 nm (left) and H_2O_2 (millimolar) accumulating in stationary-phase cultures (right) were determined. # and *, significantly different from the wild-type and Pn-*aqpC*-com strains and the respective static cultures, respectively. (K, top and middle) Ten microliters of the mid-exponential-phase cultures in panel J was spotted onto a BHI agar plate and incubated in a 5% O_2 environment for 10 h (top), and H_2O_2 was then determined (middle) as described in Materials and Methods. (Bottom) Chemical H_2O_2 with known concentrations was used as a reference. All experiments were conducted three times, and averages ± standard deviations (SD) (A, B, D, and J) or averages ± standard errors of the means (SEM) (C, E, H, and I) from one independent assay on triplicate samples are shown. For panels B to D and J, one-way ANOVA and Tukey's test were performed; for panels E, H, and I, Student's *t* test was performed ($P < 0.05$).

The substrate-selective residue Pro232 is essential for Pn-AqpC in facilitating O_2 permeation. To determine the key substrate-selective residues for Pn-AqpC in O_2 transport, alanine substitution was performed for each YVPR on the shuttle vector pDL278-Pn-*aqpC* and then transformed into the ΔPn-*aqpC* mutant to obtain the Tyr49A, Val223A, Pro232A, and Arg238A strains. The four mutants and the Pn-*aqpC*-com strain were grown in 10 ml BHI broth, and H_2O_2 yields in the stationary-phase cultures were used as a proxy for O_2 uptake. Threefold-reduced H_2O_2 yields were determined for the Pro232A mutant (0.48 ± 0.39 mM) compared with the Pn-*aqpC*-com strain (1.46 ± 0.21 mM), whereas no significant change was observed for the Tyr49A (1.38 ± 0.17 mM), Val223A (1.41 ± 0.18 mM), and Arg238A (1.27 ± 0.26 mM) strains.

Furthermore, using the oxygen microsensor Oxy meter, 1.4-fold-lower O_2 consumption for the Pro232A mutant was determined than for the wild-type and Pn-*aqpC*-com strains (Fig. 2B). The phosphorescent oxygen probe also measured 3.3- and 2.3-fold-lower O_2 consumption rates within 3 min for the Pro232A mutant than for the wild-type and Pn-*aqpC*-com strains, respectively (Fig. 2C). These results revealed that Pro232 is the key residue of Pn-AqpC in O_2 transport.

Elevated Pn-AqpC protein contents occur in aerobic cultures. Given the role of Pn-AqpC in O_2 transport, its synthesis in response to O_2 was determined. Using the photoactivated localization microscopy (PALM) superresolution imaging technique (28), numbers of Pn-AqpC proteins per cell were quantified in anaerobically, statically, and 120-rpm-shaking-grown cultures of the Pn-*aqpC*-mMaple3 strain, which carried an mMaple3 protein (29) fusion at the C terminus of Pn-*aqpC*. Figure 3A shows representative PALM images with mMaple3 fluorescence signals; each image included a 2- to 3-cell-constituted cell chain, the typical morphology of pneumococcus. PALM data analysis indicated that the average numbers of Pn-AqpC protein molecules per cell were 23 ± 10 in anaerobic, 56 ± 6 in static, and 94 ± 9 in shaking cultures (Fig. 3A). Catalase treatment did not reduce the Pn-AqpC protein numbers (41 ± 21) in static culture; thus, O_2, but not H_2O_2, seems to induce Pn-AqpC expression.

Oxygen-induced Pn-AqpC expression was further verified by the GFP reporter strain Pn-*aqpC-gfp*. GFP fluorescence intensities showed a pattern of in anaerobic culture <60 rpm shaking culture <120 rpm shaking culture (Fig. 3B), whereas neither catalase treatment of the static culture nor H_2O_2 pulsing of the anaerobic culture changed the O_2-level-related Pn-AqpC abundances (Fig. 3C). Pn-AqpC was detected exclusively in the cellular membrane fraction (Fig. 3D), confirming its membrane protein identity as predicted by TMHMM (Fig. S1B). These findings indicated that O_2 induces the synthesis of Pn-AqpC.

The absence of Pn-AqpC reduces pneumococcal resistance to H_2O_2 and NO as well as Ply release. Given that endogenous H_2O_2 assists pneumococcus in resisting oxidative stress (7), the ΔPn-*aqpC* mutant reducing H_2O_2 resistance was presumed to be due to lower H_2O_2 production. As expected, a lower MIC of H_2O_2 was determined for the ΔPn-*aqpC* mutant (5 mM) than for the wild-type strain (8 mM). Consistently, the growth of ΔPn-*aqpC* in a BHI plate containing 10 mM H_2O_2 occurred only at a 10^{-5} dilution compared with the 10^{-6} dilutions of the wild-type and Pn-*aqpC*-com strains (Fig. 4A). Moreover, only 2.3% of ΔPn-*aqpC* mutant cells survived the challenge with 10 mM H_2O_2, compared with survival rates of >40% for the wild-type and Pn-*aqpC*-com strains (Fig. 4B). However, 40 μM H_2O_2 prepulsing significantly increased 10 mM H_2O_2 survival of the ΔPn-*aqpC* mutant (Fig. 4B), indicating that Pn-AqpC-promoted endogenous H_2O_2 production makes pneumococcus withstand exogenous H_2O_2 challenge.

Next, the role of Pn-AqpC in pneumococcal resistance to NO, another oxidant, was assayed as macrophages employ NO-dependent bactericidal mechanisms to clear infecting bacteria (8). Only 5% of the ΔPn-*aqpC* cells survived 5 mM NO, compared to about 20% survival of the wild-type and Pn-*aqpC*-com strains (Fig. 4C), suggesting the involvement of Pn-AqpC in NO resistance. Given that the proteins involved in H_2O_2 resistance also assist *E. coli* in resisting NO (30), we used 40 μM H_2O_2 to prepulse the three strains. H_2O_2 prepulsing increased the NO survival of the ΔPn-*aqpC* mutant by 6-fold but had no effect on the survival of the wild-type and Pn-*aqpC*-com strains

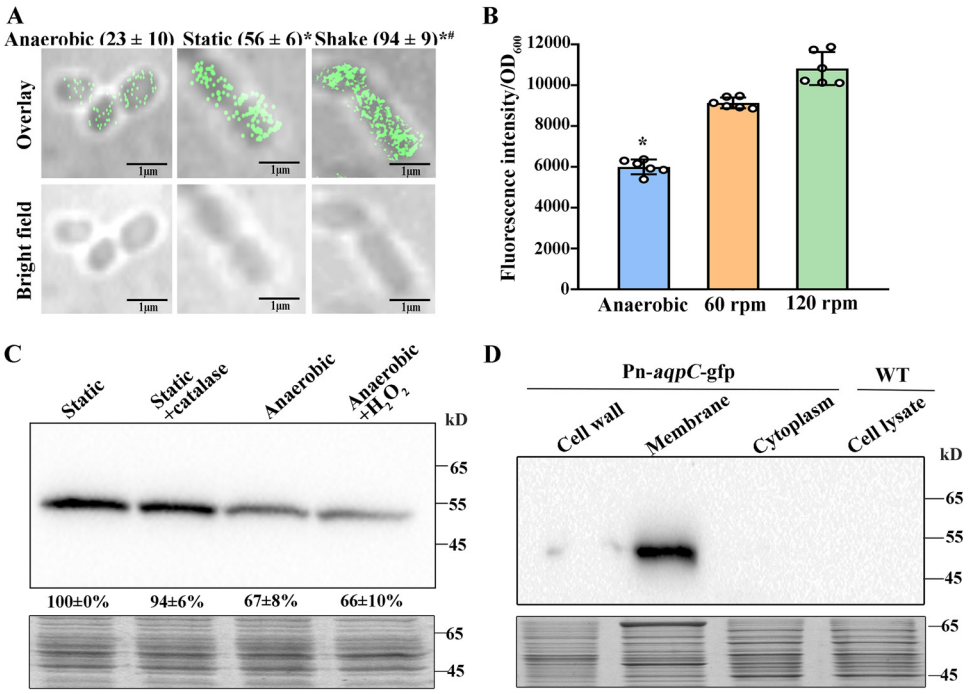

FIG 3 Oxygen induces Pn-*aqpC* expression. (A) PALM imaging to assay Pn-AqpC protein expression in the R6 Pn-AqpC-mMaple3 strain grown anaerobically, statically, or with shaking at 120 rpm with the addition of catalase. The mMaple3 fluorescence of mid-exponential-phase cells was observed after 30 min of air exposure in the dark. Pn-AqpC protein numbers were quantified in 18 representative cells, and averages ± SD per cell are shown in parentheses. * and #, significantly different from anaerobically and statically grown cells, respectively ($P < 0.05$ by one-way ANOVA with Tukey's test). (B) GFP fluorescence of the mid-exponential-phase cultures was measured in R6 Pn-*aqpC-gfp* cells cultured anaerobically and shaken with the addition of catalase after air exposure in the dark. The experiments were repeated three times, and averages ± SD from one independent experiment with sextuplicate samples are shown. *, significantly different from the shaking culture cells ($P < 0.05$ by one-way ANOVA with Tukey's test). (C, top) Western blot assay of the expression of GFP-tagged Pn-AqpC in the R6 Pn-*aqpC-gfp* strain grown statically with or without 1 kilounit (KU)/ml catalase and anaerobically with or without 40 μM H_2O_2 treatment. Band intensities were measured using ImageJ and are shown as percentages of that in static culture. Averages ± SD from three experiments are shown. (Bottom) Total protein separated on an SDS-PAGE gel and used as the protein loading control. (D, top) Statically grown Pn-*aqpC-gfp* cells were fractionated into cell wall, membrane, and cytoplasmic fractions and subjected to Western blotting using anti-GFP monoclonal antibody. The cell lysate of the wild-type strain (WT) was used as a negative control. (Bottom) SDS-PAGE gel of total protein in each fraction used as the protein loading control. Representative results from three independent experiments are shown in panels A, C, and D.

(Fig. 4C). This shows that lower H_2O_2 levels induce cross-protection of pneumococci from NO stress.

Stationary-phase cells of pneumococci are usually autolyzed and thus release Ply (31), a major virulence factor. The deletion of Pn-*aqpC* appeared to significantly alleviate cell autolysis (Fig. 4D) and so may also reduce Ply release and the hemolytic activity of pneumococcus. To test this, 12-h-post-stationary-phase spent cultures of the wild-type, Pn-*aqpC* deletion, and complemented strains were 2-fold serially diluted, and horse red blood cells were added. Complete erythrocyte lysis was observed in ≤4-fold dilutions of the wild-type and Pn-*aqpC*-com cultures, but only partial hemolysis occurred in the 2-fold-diluted ΔPn-*aqpC* culture (Fig. 4E). Consistently, about 2.3-fold less Ply protein was detected in the 12-h-post-stationary-phase spent culture of the ΔPn-*aqpC* mutant (Fig. 4F). This shows that Pn-*aqpC* deletion reduces cell lysis as well as Ply release.

Deletion of Pn-*aqpC* reduces pneumococcal survival in macrophages and damage to macrophages. Macrophages, the first line of defense of the human immune system, utilize reactive oxygen and nitrogen species to kill invading microbes (8, 9). Given the reduced H_2O_2 production of the ΔPn-*aqpC* mutant, the effect of the Pn-*aqpC* deletion on pneumococcal survival in macrophages was investigated. First, 1×10^5 macrophage RAW 264.7 cells were exposed to the nonencapsulated R6 wild-

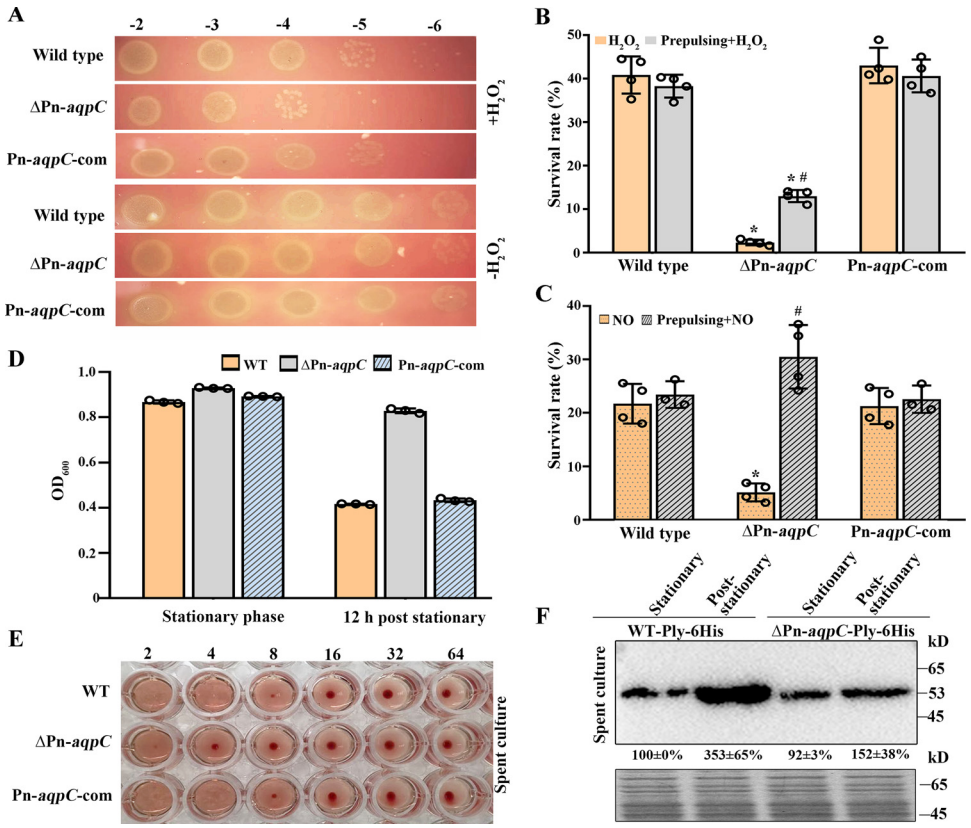

FIG 4 Absence of Pn-AqpC reduces oxidative resistance and Ply release of pneumococcus. (A) The same amounts of statically grown R6 and its derivatives were 10-fold serially diluted and spotted onto BHI agar containing 10 mM H_2O_2 or not. Representative growth results from triplicates are shown. (B and C) Strains in panel A were either directly treated or prepulsed with 40 μM H_2O_2 before being treated with 10 mM H_2O_2 (B) or 5 mM NO (C). Survival rates are calculated based on CFU. * and #, significantly different from the wild-type and complemented strains and the H_2O_2 or NO directly treated ΔPn-*aqpC* mutant, respectively ($P < 0.05$ by one-way ANOVA with Tukey's test). (D) Cell autolysis in the stationary and 12-h-post-stationary phases of the strains in panel A was assayed by measurement of the culture OD_{600}. (E) Erythrocytes were incubated with the diluted (fold indicated at the top) 12-h-post-stationary-phase spent cultures of the strains in panel D. Hemolysis was examined after 30 min of incubation at 37°C. (F) Western blot assay of Ply amounts released from the R6 wild type (WT) and the ΔPn-*aqpC* mutant. 6×His-tagged Ply was expressed in the two strains, which were cultured statically until the stationary and 12-h-post-stationary phases. (Top) The same amounts of 10-kDa ultrafiltration-concentrated cultures were separated on an SDS-PAGE gel, and anti-His antibody was used to detect 6×His-tagged Ply. Band intensities were quantified using ImageJ software, and Ply contents are shown as percentages of the WT Ply-6×His strain (100%) in the stationary-phase spent culture. (Bottom) Total proteins separated on an SDS-PAGE gel were included as a protein loading control. All experiments were executed three times, and averages ± SD from one independent assay on triplicate or quadruplicate samples are shown. Representative results from three independent experiments are shown in panels A, E, and F.

type, Pn-*aqpC* deletion, and complemented strains at a multiplicity of infection (MOI) of 100:1. After 1 h of incubation, the bacterial cells attached to and internalized into macrophages were counted, and after additional 1-h and 1.5-h incubations, surviving pneumococcal cells within macrophages were counted. Although the numbers of viable bacterial cells of the three strains all significantly decreased, 4.5- and 3-fold-lower survival rates of the ΔPn-*aqpC* mutant were determined after additional 1-h and 1.5-h incubations, respectively, than for the wild-type and Pn-*aqpC*-com strains (Fig. 5A). This validates the contribution of Pn-AqpC to pneumococcal survival in macrophages.

To query whether the reduced macrophage survival is caused by the increased NO sensitivity of the ΔPn-*aqpC* mutant, diphenyleneiodonium chloride (DPI), an inhibitor of inducible nitric oxide synthase (iNOS) (32), was used to inhibit NO production by macrophages. The addition of DPI increased the number of living cells 4.9- and 5.6-fold for the wild-type and Pn-*aqpC*-com strains, respectively, whereas it enhanced the survival of the ΔPn-*aqpC* mutant 8.4-fold in macrophages (Fig. 5A), indicating that Pn-

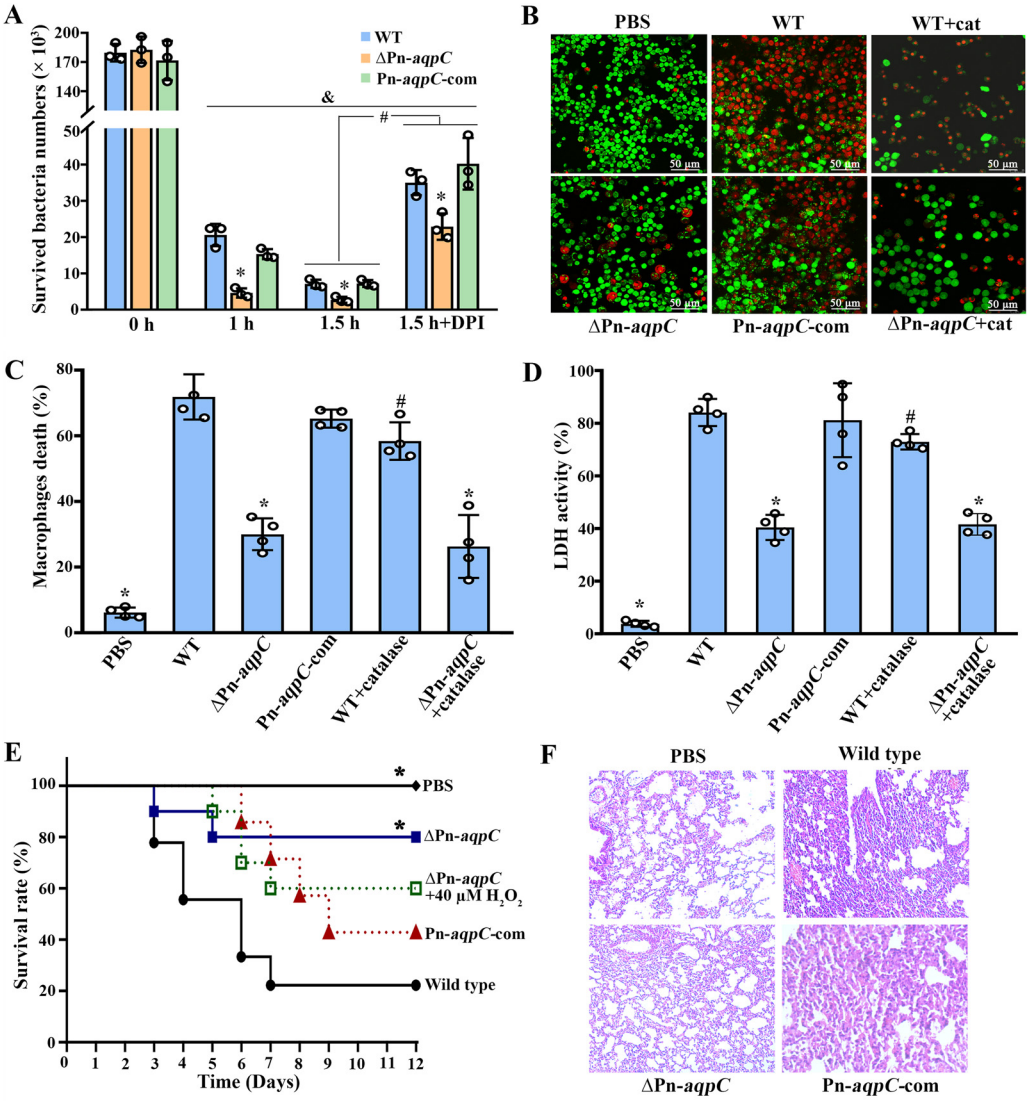

FIG 5 Deletion of Pn-*aqpC* reduces pneumococcal survival and damage to macrophages and significantly attenuates virulence to mice. (A) Pneumococcal survival in macrophages was assayed by coincubation of 1×10^5 RAW 264.7 cells with the R6 wild type (WT) and derivatives at an MOI of 100:1. After 1 h of incubation, bacterial cells in the culture were removed, those attached to and internalized in macrophages were recorded, and this time point was set as 0 h. After additional 1- and 1.5-h (total, 2- and 2.5-h) incubations in fresh medium containing antibiotics, the pneumococcal cells that survived within macrophages were counted. The nitric oxide (NO) synthetase inhibitor DPI was added to reduce NO production by macrophages. (B to D) Using the same approach as the one described above for panel A, the contribution of Pn-AqpC to R6's damage to macrophages was evaluated. (B) Live (green)/dead (red) cell staining of macrophages. The addition of 1 KU/ml catalase (cat) was used to assay the role of H_2O_2. (C) After 16 h of antibiotic treatment, macrophage death (percent) was calculated. (D) Bacterial damage to macrophages was also evaluated by leaked lactate dehydrogenase (LDH) activities. &, significantly different from the respective strains at 0 h (A); *, significantly different from the wild-type and Pn-*aqpC*-com strains; #, significantly different from that without DPI treatment (A) or the respective strain without catalase addition (C and D) ($P < 0.05$ by one-way ANOVA and Tukey's test). (E) BALB/c mice ($n = 10$; female) were intratracheally infected with 1×10^7 CFU of statically grown D39 wild-type and ΔPn-*aqpC* strains with or without 40 μM H_2O_2 pretreatment and the Pn-*aqpC*-com strain. PBS-administered mice were included as controls. Survival of the infected mice was monitored for up to 12 days, and representative survival curves from two independent experiments are shown. *, significantly different from the wild-type and Pn-*aqpC*-com strains ($P < 0.05$ by a log rank Mantel-Cox test). (F) Histopathological observation of the lung tissues of mice that survived PBS administration and ΔPn-*aqpC* infection and those that died from wild-type and Pn-*aqpC*-com infections.

AqpC-conferred pneumococcus oxidative stress resistance assists its survival in macrophages.

Given that H_2O_2 induces macrophage death (33), the role of the deletion of Pn-*aqpC* in pneumococcal damage to macrophages was examined. Upon bacterial

challenging, only 30% of macrophage cells died from coincubation with the ΔPn-*aqpC* mutant, compared to 72% and 65% cell death from coincubation with the wild-type and Pn-*aqpC*-com strains, respectively (Fig. 5B and C), whereas the addition of 1 KU/ml catalase reduced macrophage damage from the wild type by 13% (59% with versus 72% without catalase) but did not alleviate the damage from the ΔPn-*aqpC* mutant (Fig. 5B and C), indicating that Pn-AqpC-promoted H_2O_2 production has some contributions to macrophage death. The roles of Pn-AqpC and H_2O_2 in damage to macrophages were also verified by the activities of lactate dehydrogenase in the cultures leaked from macrophages (Fig. 5D). However, the catalase-treated wild-type cells still caused significantly higher macrophage death (59%) than the ΔPn-*aqpC* mutant (30%), implying that Pn-AqpC itself or other Pn-AqpC-impacted factors, possibly the reduced release of Ply, contribute to macrophages death.

Pn-AqpC is required for pneumococcal virulence in a murine pulmonary infection model. Given that H_2O_2 and Ply are major virulence factors (1, 2), and the deletion of Pn-*aqpC* not only increased the H_2O_2 and NO susceptibility of but also reduced Ply release by pneumococci, the contributions of Pn-AqpC to pneumococcal virulence were evaluated in a murine pneumonia infection model. BALB/c mice were intratracheally infected with 1.0×10^7 CFU of D39, its Pn-*aqpC* deletion mutant (pretreated with or without 40 μM H_2O_2), and the Pn-*aqpC*-com strain. By monitoring mouse survival for 12 days postinfection, we found that the Pn-*aqpC* deletion significantly enhanced mouse survival to 78%, compared with 22% and 43% survival rates in the wild-type- and Pn-*aqpC*-com-infected groups, respectively (Fig. 5E), indicating that Pn-AqpC is involved in pneumococcal pathogenicity. Of note, the survival rate of mice infected with the 40 μM H_2O_2-pretreated ΔPn-*aqpC* mutant was reduced to 60%, compared with 78% survival of those infected by the non-H_2O_2-pretreated ΔPn-*aqpC* strain, suggesting that low-H_2O_2-induced oxidative resistance enhances pneumococcal pathogenicity in addition to other virulence factors.

Neither was inflammatory cell immersion (Fig. 5F) observed nor were pneumococci recovered from the lung tissue of the surviving mice infected by the ΔPn-*aqpC* mutant, whereas $1.35 \times 10^8 \pm 0.91 \times 10^8$ and $1.54 \times 10^8 \pm 0.72 \times 10^8$ CFU/ml of pneumococci were recovered from the lungs of dead mice infected by the D39 wild-type and Pn-*aqpC*-com strains, respectively. These data confirmed the contribution of Pn-AqpC to pneumococcal pathogenicity.

DISCUSSION

To date, 13 and 120 aquaporin isoforms have been identified in humans and plants, respectively, and are delineated into three major subfamilies: the classical water-transporting aquaporins, glycerol-transporting aquaglyceroporins, and AQP supergene channel superaquaporins (14, 15, 34). They facilitate the transmembrane diffusion of water, glycerol, H_2O_2, CO_2, and other small uncharged solutes (14–16, 26, 34, 35). Here, we report a new aquaporin subfamily represented by pneumococcal Pn-AqpC, which functions as an oxygen porin to facilitate oxygen uptake. Phylogenetically, the oxygen porins are distantly related to aquaglyceroporins and possess substrate-selective amino acid residues distinct from those of aquaporins and aquaglyceroporins. Importantly, the oxygen porin Pn-AqpC contributes significantly to the pathogenicity of *S. pneumoniae*. As depicted in Fig. 6, pneumococcal Pn-AqpC, which is increasingly synthesized under conditions of higher O_2 contents, facilitates O_2 influx into cells and thus promotes H_2O_2 production by pneumococcus. Endogenous H_2O_2 helps pneumococci adapt to higher exogenous H_2O_2 and NO levels; therefore, the deletion of Pn-*aqpC* reduced the H_2O_2 and NO resistance of pneumococci. Accordingly, the presence of Pn-AqpC promotes pneumococcal survival in macrophages and possibly other host immune cells. In addition, the absence of Pn-AqpC alleviates pneumococcal autolysis and, thus, Ply release and significantly reduces pneumococcal damage to macrophages. In support of this, the absence of Pn-AqpC significantly attenuated the virulence of pneumococcus in a murine pneumonia model. Thus, the new subfamily of prokaryotic aquaporins, represented by Pn-AqpC, might be virulence-related proteins.

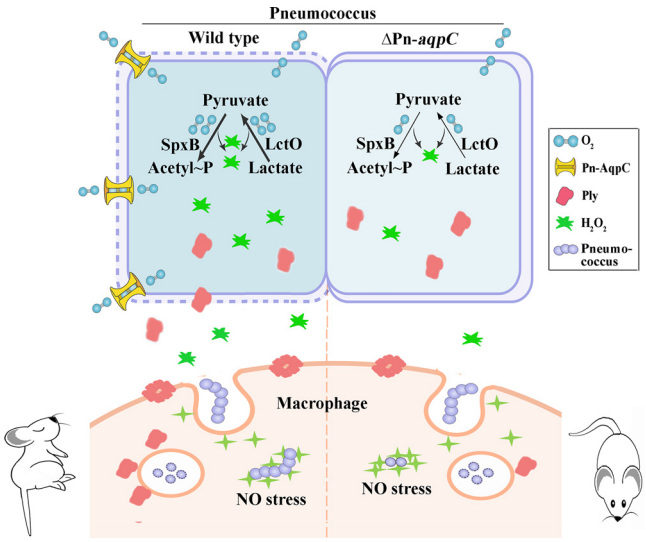

FIG 6 The newly identified oxygen-facilitating aquaporin Pn-AqpC modulates H_2O_2 production, ROS and RNS resistance, and pneumolysin (Ply) release and contributes significantly to the pathogenicity of pneumococcus. Pn-AqpC, an atypical aquaglyceroporin, functions as an oxygen porin to facilitate O_2 influx and promotes pneumococcus to produce H_2O_2 via pyruvate oxidase (SpxB) and lactate oxidase (LctO). Endogenous H_2O_2 endows but deletion of Pn-*aqpC* reduces pneumococcus resistance to higher exogenous H_2O_2 and NO levels; therefore, the presence of Pn-AqpC enhances the survival of pneumococci in macrophages. Additionally, the presence of Pn-AqpC promotes pneumococcal cell lysis and, thus, Ply release. As the pneumococcal hemolysin Ply perforates eukaryotic cellular membranes and induces macrophage necroptosis, the presence of Pn-AqpC enhances pneumococcal damage to macrophages. Consistently, the absence of Pn-AqpC significantly attenuates the virulence of *S. pneumoniae* in a murine pneumonia model.

To our knowledge, Pn-AqpC is the first reported oxygen porin with defined physiological functions. Although O_2 freely diffuses across the cytoplasmic membrane (36), assays of both *in vivo* and heterogeneously expressed yeast and *in vitro*-reconstituted proteoliposomes all determined that Pn-AqpC increases O_2 flux across the cellular membrane (Fig. 2), particularly when pneumococci are grown under lower O_2 levels (Fig. 2J and K) similar to those in most host environments (11). In addition, the pneumococcal cellular membrane appears to have lower O_2 permeability than that of *E. coli*, highlighting the role of Pn-AqpC in pneumococci, which could require controllable O_2 influx for H_2O_2 synthesis. Enhanced Pn-AqpC contents were found in aerobically grown pneumococcus (Fig. 3), conforming to its oxygen facilitator mission; however, similar Pn-*aqpC* transcript levels were found in aerobic and anaerobic cultures (data not shown), implying the posttranscriptional regulation of Pn-AqpC expression. So far, an O_2-facilitating function has been reported only for human AQP1 and *Nicotiana tabacum* PIP1;3 when ectopically expressed in yeast (26). They are affiliated with water-type aquaporins and distantly related to Pn-AqpC at very low protein identities (20% and 14%, respectively) and distinct selective filter residues; therefore, prokaryotic Pn-AqpC represents a novel subfamily of aquaporins. Analogous to other aquaporin orthologs, Pn-AqpC forms a tetramer, as indicated by structural homology modeling implemented in SWISS-MODEL (Fig. S2A) and a macromolecular aggregate formed by the purified Pn-AqpC–10×His protein (Fig. 2F and G). Although O_2 is predicted to permeate through the central pore of the four monomers of human AQP1 (36), Pro232 in the Pn-AqpC ar/R region has been determined to be crucial for facilitating O_2 transport (Fig. 2B and C). Thus, O_2 could be transported through the oxygen porin substrate channel in addition to the tetramer central pore. Thus far, only O_2, but neither H_2O nor glycerol and H_2O_2, has been verified as the substrate of Pn-AqpC (Fig. 2; see also Fig. S3 in the supplemental material). Of note, distinct from most other reported aquaporins, Pn-AqpC does not contain cysteine residues and thus is not inactivated by mercury chloride (data not shown).

Significantly, the oxygen porin Pn-AqpC contributes to pneumococcal pathogenicity, as the deletion of Pn-*aqpC* markedly attenuated lethality to mice (Fig. 5E). Through an exhaustive search, Pn-*aqpC* orthologs were found in all 8,183 pneumococcal genomes and contigs, which are attributed to 77 capsular serotypes and capsule-free strains. These orthologs exhibit 97% to 100% amino acid sequence identities with Pn-AqpC and 100% identity of YVPR in the ar/R region (Fig. 1C; Data Set S1). Additionally, Pn-AqpC orthologs are widely distributed among members of the genera *Streptococcus* and *Lactococcus* of the *Streptococcaceae* family, the genera *Lactobacillus* and *Pediococcus* of the *Lactobacillaceae* family, the genera *Oenococcus* and *Weissella* of the *Leuconostocaceae* family, and the genus *Enterococcus* of the *Enterococcaceae* family (Fig. 1C), so the members of this aquaporin subfamily appear to be restrictively present in facultative anaerobic bacteria, implying that they could contribute to the oxidative adaptation of these bacteria through O_2 influx-enabled endogenous H_2O_2 production. Of note, Pn-AqpC orthologs are particularly prominent in some pathogenic streptococcal species, such as *Streptococcus pyogenes* and *S. mutans* (Fig. 1A), implying their association with virulence. Although the non-H_2O_2-producing species *S. mutans* also possesses a Pn-AqpC ortholog (SMU_396), its O_2-facilitating role is not likely involved in H_2O_2 production through oxidases, whereas *S. mutans* encodes H_2O-forming NADH oxidase (Nox), which uses O_2 to oxidize NADH to NAD^+ to achieve cellular redox balance and energy production (37). Deletion of the *nox* gene reduced O_2 consumption by pneumococcus. A previous study also found that O_2 promotes O_2-tolerant *S. mutans* growth (38); thus, *S. mutans* AqpC could also have an important physiological role.

Based on the experimental evidence of pneumococcal survival in and damage to macrophages (Fig. 5A to D), we hypothesize that the mechanistic basis of Pn-AqpC in pneumococcal pathogenicity lies in its control of pneumococcal H_2O_2 production and Ply release. Compared with other pathogenic bacteria, streptococci are highly capable of resisting oxidative stress via endogenous H_2O_2-induced resistance to higher levels of exogenous H_2O_2 (6, 39), and this unique characteristic enables them to defend against the innate immune system of the infected host (9). H_2O_2 also contributes to pneumococcal virulence by damaging alveolar epithelial cell DNA and suppressing host innate immune systems (4, 5). Consistently, the major H_2O_2-producing enzyme pyruvate oxidase is crucial for the virulence of *S. pneumoniae* (40). This work identified that Pn-AqpC, by facilitating O_2 uptake, acts as a novel key component in controlling H_2O_2 production and oxidative stress resistance; thus, the absence of this membrane protein causes *S. pneumoniae* to be rapidly eliminated by macrophages and reduces damage to macrophages. Survival in macrophages could be important for pneumococcal invasion and is critical for pneumococcal bacteremia and persistence within hosts (10, 41). Remarkably, the presence of Pn-AqpC elevates pneumococcal autolysis and Ply release (Fig. 4E and F), probably due to endogenous H_2O_2 production, thus increasing the hemolytic activity of pneumococci. Ply, as the major virulence factor of pneumococci, has been known to mediate bacterial transmission, trigger inflammatory responses, and cause macrophage necrosis (3, 42, 43). Rapid autolysis and pneumolysin release were reported to increase the pathogenicity of pneumococcal serotype 1 (44). In addition, no correlations have been found between Pn-AqpC and other identified pneumococcal virulence factors, as the deletion of Pn-*aqpC* did not alter the transcription of *lytA*, *psaA*, *pspC*, *spxB*, and *lctO* (Fig. S4) or the capsule polysaccharide amounts (Fig. S6). Therefore, the virulence relevance of Pn-AqpC lies mainly in its oxygen-transporting function.

Collectively, Pn-AqpC, by facilitating O_2 uptake, modulates H_2O_2 production and Ply release, the two major virulence factors of pneumococci, and contributes remarkably to pneumococcal virulence. Pn-*aqpC* orthologs were found in all 8,183 pneumococcal genomes and contigs (Data Set S1). Therefore, the conserved membrane-integrated Pn-AqpC is exposed as a new potential target for fighting against pneumococcal disease.

MATERIALS AND METHODS

Experimental strains and growth. Experimental strains are listed in Table S2 in the supplemental material. Pneumococcus was grown in brain heart infusion (BHI) broth or agar plates (BD Difco) with 5%

sterile defibrinated sheep blood at 37°C with 5% CO_2. Pneumococcal strains were grown statically, with shaking, or anaerobically under 100% nitrogen. When required, kanamycin (1 mg/ml) and spectinomycin (300 μg/ml) were added.

Construction of genetically modified strains. All primers are listed in Table S2. The PCR ligation method (45) was used to construct the Pn-*aqpC* and *nox* deletion strains and His-, photoactivatable fluorescent protein mMaple3 (29)-, or super folder green fluorescent protein (sfGFP)-tagged strains of *S. pneumoniae*. The spectinomycin and kanamycin resistance genes were derived from plasmids pDL278 (46) and pALH124 (47), respectively. The Pn-*aqpC* gene with its promoter was cloned into pDL278 for complemented strain construction. Alanine substitutions for Tyr49, Val223, Pro232, and Arg238 were implemented on pDL278-Pn-*aqpC* using a site-directed gene mutagenesis kit (Beyotime, China). Transformation was performed as described previously (48). Correct transformants were confirmed by PCR and DNA sequencing.

Test of the transportable substrates of Pn-AqpC-constituted proteoliposomes. The purified 10×His-tagged Pn-AqpC protein was reconstituted into liposomes made by the *S. pneumoniae* cellular membrane lipid (49, 50) and *E. coli* total lipid extract (Avanti) as previously described (16, 27). Detailed procedures are available in Text S1 in the supplemental material.

To examine the O_2 permeability of Pn-AqpC, cell membrane-impermeable and oxygen-quenchable phosphorescent oxygen probes (Cayman Chemical) were encapsulated into proteoliposomes and Pn-AqpC-devoid liposomes. The proteoliposomes and liposomes were vacuumed and N_2 gas flushed for 7 cycles, and 100 μl per well was then dispersed into a 96-well plate (Corning) under air. The fluorescence intensity of the phosphorescent oxygen probe was monitored (excitation at 380 nm and emission at 650 nm) for a recommended delay of 30 μs using a Synergy H4 hybrid multimode microplate reader (BioTek). Water and glycerol permeabilities were assayed using an SX20 stopped-flow spectrometer as previously described (27, 51). The experiments were repeated three times.

PALM imaging. Mid-exponential-phase Pn-*aqpC*-mMaple3 cells were exposed to air for 30 min in the dark and then observed using PALM imaging (28) as previously described (12). The superresolution images were constructed using Insight3 software (52), which was kindly provided by Bo Huang (University of California, San Francisco). PALM data analyses such as drift correction, protein abundance, and image rendering were carried out using custom-written Matlab scripts.

Assay of pneumococcal survival in macrophages and damage to macrophages. Mouse monocyte-macrophage RAW 264.7 cells (1×10^5) were challenged for 1 h with pneumococcus at a multiplicity of infection of 100:1. After removing the bacteria, macrophages were incubated for another 1 and 1.5 h to count CFU of pneumococci within macrophages or for 16 h to determine macrophage death. Detailed procedures are available in Text S1 in the supplemental material.

***In vivo* mouse infection experiment.** BALB/c mice (specific-pathogen-free [SPF] grade) were purchased from Vital River Company (Beijing, China). Animal experiments were approved by the Biomedical Research Ethics Committee of the Institute of Microbiology, Chinese Academy of Sciences. The protocol was approved by the Institutional Animal Care and Use Committee. *S. pneumoniae* D39 and derivative strains were intratracheally administered to 6- to 8-week-old female BALB/c mice at 1×10^7 CFU in 20 μl phosphate-buffered saline (PBS), and PBS-administered BALB/c mice were included as controls. Mouse survival (10 per group) was monitored for 12 days. Mice were sacrificed under anesthesia, half-lungs were ground for enumerating pneumococcal CFU, and the other halves were used for histopathological observation.

Statistical analysis. One-way analysis of variance (ANOVA) followed by Tukey's *post hoc* test and Student's *t* test was performed using PASW Statistics 18 and Excel, respectively. A log rank Mantel-Cox test was performed using GraphPad Prism 8.0. The level of significance was determined at a *P* value of <0.05.

Other procedures. Detailed procedures are available in Text S1 in the supplemental material.

SUPPLEMENTAL MATERIAL

Supplemental material is available online only.

TEXT S1, DOCX file, 0.04 MB.

FIG S1, TIF file, 1 MB.

FIG S2, TIF file, 2.3 MB.

FIG S3, TIF file, 1.8 MB.

FIG S4, TIF file, 0.1 MB.

FIG S5, TIF file, 1.3 MB.

FIG S6, TIF file, 0.7 MB.

TABLE S1, DOCX file, 0.02 MB.

TABLE S2, DOCX file, 0.03 MB.

DATA SET S1, XLSX file, 1.9 MB.

ACKNOWLEDGMENTS

This study was supported by the National Natural Science Foundation of China (no. 31970035).

We thank Jinghua Yang and Dongdong Zhao at the Institute of Microbiology, CAS, for technical assistance in cytology and animal experiments, respectively; Yun Zhu at Peking University for assistance in PALM imaging; Xiaolan Zhang at the Institute of Microbiology, CAS, for help in confocal laser scanning microscopy imaging; and Jie Feng and Na Tang at the Institute of Microbiology, CAS, for help in searching Pn-AqpC homologs in the NCBI *S. pneumoniae* genome and contig sequence databases.

Q.H. and H.T. conducted most bacterial and cytological experiments; Q.H., H.T., J.W., and P.G. performed mouse pneumonia model experiments; L.Z. determined the growth of pneumococci and conducted some genetic experiments; C.L. and J.Z. edited the paper; and H.T. and X.D. designed the experiments and wrote the paper.

We declare no competing interests.

REFERENCES

1. Weiser JN, Ferreira DM, Paton JC. 2018. *Streptococcus pneumoniae*: transmission, colonization and invasion. Nat Rev Microbiol 16:355–367. https://doi.org/10.1038/s41579-018-0001-8.
2. Kadioglu A, Weiser JN, Paton JC, Andrew PW. 2008. The role of *Streptococcus pneumoniae* virulence factors in host respiratory colonization and disease. Nat Rev Microbiol 6:288–301. https://doi.org/10.1038/nrmicro1871.
3. Zafar MA, Wang Y, Hamaguchi S, Weiser JN. 2017. Host-to-host transmission of *Streptococcus pneumoniae* is driven by its inflammatory toxin, pneumolysin. Cell Host Microbe 21:73–83. https://doi.org/10.1016/j.chom.2016.12.005.
4. Rai P, Parrish M, Tay IJ, Li N, Ackerman S, He F, Kwang J, Chow VT, Engelward BP. 2015. *Streptococcus pneumoniae* secretes hydrogen peroxide leading to DNA damage and apoptosis in lung cells. Proc Natl Acad Sci U S A 112:E3421–E3430. https://doi.org/10.1073/pnas.1424144112.
5. Erttmann SF, Gekara NO. 2019. Hydrogen peroxide release by bacteria suppresses inflammasome-dependent innate immunity. Nat Commun 10:3493. https://doi.org/10.1038/s41467-019-11169-x.
6. Lisher JP, Tsui H-CT, Ramos-Montanez S, Hentchel KL, Martin JE, Trinidad JC, Winkler ME, Giedroc DP. 2017. Biological and chemical adaptation to endogenous hydrogen peroxide production in *Streptococcus pneumoniae* D39. mSphere 2:e00291-16. https://doi.org/10.1128/mSphere.00291-16.
7. Pericone CD, Park S, Imlay JA, Weiser JN. 2003. Factors contributing to hydrogen peroxide resistance in *Streptococcus pneumoniae* include pyruvate oxidase (SpxB) and avoidance of the toxic effects of the Fenton reaction. J Bacteriol 185:6815–6825. https://doi.org/10.1128/JB.185.23.6815-6825.2003.
8. Kerr AR, Wei XQ, Andrew PW, Mitchell TJ. 2004. Nitric oxide exerts distinct effects in local and systemic infections with *Streptococcus pneumoniae*. Microb Pathog 36:303–310. https://doi.org/10.1016/j.micpath.2004.02.001.
9. Fang FC. 2004. Antimicrobial reactive oxygen and nitrogen species: concepts and controversies. Nat Rev Microbiol 2:820–832. https://doi.org/10.1038/nrmicro1004.
10. Ercoli G, Fernandes VE, Chung WY, Wanford JJ, Thomson S, Bayliss CD, Straatman K, Crocker PR, Dennison A, Martinez-Pomares L, Andrew PW, Moxon ER, Oggioni MR. 2018. Intracellular replication of *Streptococcus pneumoniae* inside splenic macrophages serves as a reservoir for septicaemia. Nat Microbiol 3:600–610. https://doi.org/10.1038/s41564-018-0147-1.
11. Yesilkaya H, Andisi VF, Andrew PW, Bijlsma JJ. 2013. *Streptococcus pneumoniae* and reactive oxygen species: an unusual approach to living with radicals. Trends Microbiol 21:187–195. https://doi.org/10.1016/j.tim.2013.01.004.
12. Tong H, Wang X, Dong Y, Hu Q, Zhao Z, Zhu Y, Dong L, Bai F, Dong X. 2019. A *Streptococcus* aquaporin acts as peroxiporin for efflux of cellular hydrogen peroxide and alleviation of oxidative stress. J Biol Chem 294:4583–4595. https://doi.org/10.1074/jbc.RA118.006877.
13. Preston GM, Carroll TP, Guggino WB, Agre P. 1992. Appearance of water channels in *Xenopus* oocytes expressing red cell CHIP28 protein. Science 256:385–387. https://doi.org/10.1126/science.256.5055.385.
14. Ishibashi K, Morishita Y, Tanaka Y. 2017. The evolutionary aspects of aquaporin family. Adv Exp Med Biol 969:35–50. https://doi.org/10.1007/978-94-024-1057-0_2.
15. Tesse A, Grossini E, Tamma G, Brenner C, Portincasa P, Marinelli RA, Calamita G. 2018. Aquaporins as targets of dietary bioactive phytocompounds. Front Mol Biosci 5:30. https://doi.org/10.3389/fmolb.2018.00030.
16. Borgnia MJ, Agre P. 2001. Reconstitution and functional comparison of purified GlpF and AqpZ, the glycerol and water channels from *Escherichia coli*. Proc Natl Acad Sci U S A 98:2888–2893. https://doi.org/10.1073/pnas.051628098.
17. Rodrigues O, Reshetnyak G, Grondin A, Saijo Y, Leonhardt N, Maurel C, Verdoucq L. 2017. Aquaporins facilitate hydrogen peroxide entry into guard cells to mediate ABA- and pathogen-triggered stomatal closure. Proc Natl Acad Sci U S A 114:9200–9205. https://doi.org/10.1073/pnas.1704754114.
18. Wang Y, Li R, Li D, Jia X, Zhou D, Li J, Lyi SM, Hou S, Huang Y, Kochian LV, Liu J. 2017. NIP1;2 is a plasma membrane-localized transporter mediating aluminum uptake, translocation, and tolerance in *Arabidopsis*. Proc Natl Acad Sci U S A 114:5047–5052. https://doi.org/10.1073/pnas.1618557114.
19. Calamita G, Perret J, Delporte C. 2018. Aquaglyceroporins: drug targets for metabolic diseases? Front Physiol 9:851. https://doi.org/10.3389/fphys.2018.00851.
20. Savage DF, O'Connell JD, III, Miercke LJW, Finer-Moore J, Stroud RM. 2010. Structural context shapes the aquaporin selectivity filter. Proc Natl Acad Sci U S A 107:17164–17169. https://doi.org/10.1073/pnas.1009864107.
21. Tong H, Hu Q, Zhu L, Dong X. 2019. Prokaryotic aquaporins. Cells 8:1316. https://doi.org/10.3390/cells8111316.
22. Calamita G, Kempf B, Bonhivers M, Bishai WR, Bremer E, Agre P. 1998. Regulation of the *Escherichia coli* water channel gene *aqpZ*. Proc Natl Acad Sci U S A 95:3627–3631. https://doi.org/10.1073/pnas.95.7.3627.
23. Paton JC. 1996. The contribution of pneumolysin to the pathogenicity of *Streptococcus pneumoniae*. Trends Microbiol 4:103–106. https://doi.org/10.1016/0966-842X(96)81526-5.
24. Belousov VV, Fradkov AF, Lukyanov KA, Staroverov DB, Shakhbazov KS, Terskikh AV, Lukyanov S. 2006. Genetically encoded fluorescent indicator for intracellular hydrogen peroxide. Nat Methods 3:281–286. https://doi.org/10.1038/nmeth866.
25. Auzat I, Chapuy-Regaud S, Le Bras G, Dos Santos D, Ogunniyi AD, Le Thomas I, Garel JR, Paton JC, Trombe MC. 1999. The NADH oxidase of *Streptococcus pneumoniae*: its involvement in competence and virulence. Mol Microbiol 34:1018–1028. https://doi.org/10.1046/j.1365-2958.1999.01663.x.
26. Zwiazek JJ, Xu H, Tan X, Navarro-Rodenas A, Morte A. 2017. Significance of oxygen transport through aquaporins. Sci Rep 7:40411. https://doi.org/10.1038/srep40411.
27. Borgnia MJ, Kozono D, Calamita G, Maloney PC, Agre P. 1999. Functional reconstitution and characterization of AqpZ, the *E. coli* water channel protein. J Mol Biol 291:1169–1179. https://doi.org/10.1006/jmbi.1999.3032.
28. Betzig E, Patterson GH, Sougrat R, Lindwasser OW, Olenych S, Bonifacino JS, Davidson MW, Lippincott-Schwartz J, Hess HF. 2006. Imaging intracellular fluorescent proteins at nanometer resolution. Science 313:1642–1645. https://doi.org/10.1126/science.1127344.
29. Wang S, Moffitt JR, Dempsey GT, Xie XS, Zhuang X. 2014. Characterization and development of photoactivatable fluorescent proteins for single-molecule-based superresolution imaging. Proc Natl Acad Sci U S A 111:8452–8457. https://doi.org/10.1073/pnas.1406593111.
30. Hausladen A, Privalle CT, Keng T, DeAngelo J, Stamler JS. 1996. Nitrosative stress: activation of the transcription factor OxyR. Cell 86:719–729. https://doi.org/10.1016/s0092-8674(00)80147-6.
31. Mitchell TJ, Dalziel CE. 2014. The biology of pneumolysin. Subcell Biochem 80:145–160. https://doi.org/10.1007/978-94-017-8881-6_8.
32. Gryllos I, Grifantini R, Colaprico A, Cary ME, Hakansson A, Carey DW, Suarez-Chavez M, Kalish LA, Mitchell PD, White GL, Wessels MR. 2008. PerR confers

phagocytic killing resistance and allows pharyngeal colonization by group A *Streptococcus*. PLoS Pathog 4:e1000145. https://doi.org/10.1371/journal.ppat.1000145.
33. Okahashi N, Nakata M, Kuwata H, Kawabata S. 2016. *Streptococcus oralis* induces lysosomal impairment of macrophages via bacterial hydrogen peroxide. Infect Immun 84:2042–2050. https://doi.org/10.1128/IAI.00134-16.
34. Maurel C, Verdoucq L, Luu DT, Santoni V. 2008. Plant aquaporins: membrane channels with multiple integrated functions. Annu Rev Plant Biol 59:595–624. https://doi.org/10.1146/annurev.arplant.59.032607.092734.
35. Uehlein N, Lovisolo C, Siefritz F, Kaldenhoff R. 2003. The tobacco aquaporin NtAQP1 is a membrane CO_2 pore with physiological functions. Nature 425:734–737. https://doi.org/10.1038/nature02027.
36. Wang Y, Cohen J, Boron WF, Schulten K, Tajkhorshid E. 2007. Exploring gas permeability of cellular membranes and membrane channels with molecular dynamics. J Struct Biol 157:534–544. https://doi.org/10.1016/j.jsb.2006.11.008.
37. Baker JL, Derr AM, Karuppaiah K, MacGilvray ME, Kajfasz JK, Faustoferri RC, Rivera-Ramos I, Bitoun JP, Lemos JA, Wen ZT, Quivey RG, Jr. 2014. *Streptococcus mutans* NADH oxidase lies at the intersection of overlapping regulons controlled by oxygen and NAD^+ levels. J Bacteriol 196:2166–2177. https://doi.org/10.1128/JB.01542-14.
38. Higuchi M. 1984. The effect of oxygen on the growth and mannitol fermentation of *Streptococcus mutants*. J Gen Microbiol 130:1819–1826. https://doi.org/10.1099/00221287-130-7-1819.
39. Tong H, Dong Y, Wang X, Hu Q, Yang F, Yi M, Deng H, Dong X. 2020. Redox-regulated adaptation of *Streptococcus oligofermentans* to hydrogen peroxide stress. mSystems 5:e00006-20. https://doi.org/10.1128/mSystems.00006-20.
40. Spellerberg B, Cundell DR, Sandros J, Pearce BJ, Idanpaan-Heikkila I, Rosenow C, Masure HR. 1996. Pyruvate oxidase, as a determinant of virulence in *Streptococcus pneumoniae*. Mol Microbiol 19:803–813. https://doi.org/10.1046/j.1365-2958.1996.425954.x.
41. Subramanian K, Henriques-Normark B, Normark S. 2019. Emerging concepts in the pathogenesis of the *Streptococcus pneumoniae*: from nasopharyngeal colonizer to intracellular pathogen. Cell Microbiol 21:e13077. https://doi.org/10.1111/cmi.13077.
42. Malley R, Henneke P, Morse SC, Cieslewicz MJ, Lipsitch M, Thompson CM, Kurt-Jones E, Paton JC, Wessels MR, Golenbock DT. 2003. Recognition of pneumolysin by Toll-like receptor 4 confers resistance to pneumococcal infection. Proc Natl Acad Sci U S A 100:1966–1971. https://doi.org/10.1073/pnas.0435928100.
43. Gonzalez-Juarbe N, Gilley RP, Hinojosa CA, Bradley KM, Kamei A, Gao G, Dube PH, Bergman MA, Orihuela CJ. 2015. Pore-forming toxins induce macrophage necroptosis during acute bacterial pneumonia. PLoS Pathog 11:e1005337. https://doi.org/10.1371/journal.ppat.1005337.
44. Jacques LC, Panagiotou S, Baltazar M, Senghore M, Khandaker S, Xu R, Bricio-Moreno L, Yang M, Dowson CG, Everett DB, Neill DR, Kadioglu A. 2020. Increased pathogenicity of pneumococcal serotype 1 is driven by rapid autolysis and release of pneumolysin. Nat Commun 11:1892. https://doi.org/10.1038/s41467-020-15751-6.
45. Liu L, Tong H, Dong X. 2012. Function of the pyruvate oxidase-lactate oxidase cascade in interspecies competition between *Streptococcus oligofermentans* and *Streptococcus mutans*. Appl Environ Microbiol 78:2120–2127. https://doi.org/10.1128/AEM.07539-11.
46. Podbielski A, Spellerberg B, Woischnik M, Pohl B, Lutticken R. 1996. Novel series of plasmid vectors for gene inactivation and expression analysis in group A streptococci (GAS). Gene 177:137–147. https://doi.org/10.1016/0378-1119(96)84178-3.
47. Liu Y, Zeng L, Burne RA. 2009. AguR is required for induction of the *Streptococcus mutans* agmatine deiminase system by low pH and agmatine. Appl Environ Microbiol 75:2629–2637. https://doi.org/10.1128/AEM.02145-08.
48. Li G, Liang Z, Wang X, Yang Y, Shao Z, Li M, Ma Y, Qu F, Morrison DA, Zhang JR. 2016. Addiction of hypertransformable pneumococcal isolates to natural transformation for in vivo fitness and virulence. Infect Immun 84:1887–1901. https://doi.org/10.1128/IAI.00097-16.
49. Trombe MC, Laneelle MA, Laneelle G. 1979. Lipid composition of aminopterin-resistant and sensitive strains of *Streptococcus pneumoniae*. Effect of aminopterin inhibition. Biochim Biophys Acta 574:290–300. https://doi.org/10.1016/0005-2760(79)90010-9.
50. Hosek T, Bougault CM, Lavergne JP, Martinez D, Ayala I, Fenel D, Restelli M, Morlot C, Habenstein B, Grangeasse C, Simorre JP. 2020. Structural features of the interaction of MapZ with FtsZ and membranes in *Streptococcus pneumoniae*. Sci Rep 10:4051. https://doi.org/10.1038/s41598-020-61036-9.
51. Heller KB, Lin EC, Wilson TH. 1980. Substrate specificity and transport properties of the glycerol facilitator of *Escherichia coli*. J Bacteriol 144:274–278. https://doi.org/10.1128/jb.144.1.274-278.1980.
52. Huang B, Wang W, Bates M, Zhuang X. 2008. Three-dimensional super-resolution imaging by stochastic optical reconstruction microscopy. Science 319:810–813. https://doi.org/10.1126/science.1153529.